INTERNATIONAL JOURNAL OF SUSTAINABLE CONSTRUCTION ENGINEERING AND TECHNOLOGY
VOL. 14 NO. 5 (2023) 196-207

IJSCET

http://publisher.uthm.edu.my/ojs/index.php/ijscet

ISSN : 2180-3242 e-ISSN : 2600-7959

International Journal of Sustainable Construction Engineering and Technology

Field and Laboratory Investigation of a 60-Year-Old Precast Prestressed Concrete Building in Japan

Nadia Kamaruddin[1*], Mohammad Mahdi Raouffard[2], Minehiro Nishiyama[3]

[1]School of Real Estate and Building Surveying, College of Built Environment, Universiti Teknologi MARA (UiTM), Shah Alam, Selangor, 40450, MALAYSIA

[2]Taisei Corporation, Structural Design, Tokyo, 1630606, JAPAN

[3]Department of Architecture and Architectural Engineering, Graduate School of Engineering, Kyoto University, Kyoto, 6158540, JAPAN

*Corresponding Author

DOI: https://doi.org/10.30880/ijscet.2023.14.05.015
Received 29 May 2023; Accepted 03 August 2023; Available online 31 October 2023

Abstract: In Japan, the application of the prestressed concrete (PC) system has become quite popular, especially in bridge and building constructions. Since it was first introduced in the early 1950s, the number of buildings using the PC system has substantially increased. However, following a certain period in the service life of the PC system, the serviceability of such structures especially following an earthquake has become a primary concern, especially when exposed to severe corrosion-prone environments. In this research, the City Hall building of Nandan Town, Awaji Island in Japan, was chosen to investigate the influence of corrosion on the durability of the building structure, which was initially constructed in 1957 as the first building that used PC members for beams. This paper describes the building and results of the field crack inspection and corrosion test results on concrete core samples from the building. Accordingly, the study found that the building had material deteriorations due to its corrosive surrounding environment and severe damage on the concrete cover of the PC anchorage.

Keywords: Durability, material deterioration, prestress concrete, precast concrete, reinforced concrete

1. Introduction

A concrete building structure that is designed and constructed according to the required standards and code specifications must be durable to withstand corrosive environments, maintaining its primary structural performance over time. However, concrete and steel materials can undergo severe physiochemical changes when exposed to corrosive-prone environments during a specific period. The occurrence of the material changes as mentioned above, as a function of time, is known as material deterioration (Li et al., 2008; Zhu & François, 2014; Hamada et al., 2003; Gao et al., 2019; Sosa, 2011). Moreover, the term deterioration of reinforced concrete (RC) elements in this study has been adapted to the corrosion of steel reinforcement as a result of severe chemical and physical changes in cover concrete, such as concrete carbonation, chloride ingress, sulfate attack, and alkali-silica reaction.

Similarly, physical changes may also range from hairline cracks to significant cover concrete spalling that exposes the reinforcement to the outer elements. As such, the structural performance of a deteriorated RC member could significantly decrease its structural stability even under gravity loads. A conceptual relationship between material deterioration and the degradation of structural performance is schematically illustrated in Fig. 1. As shown in the figure, as deterioration increases between the initiation stage and acceleration stage, structural performance decreases.

*Corresponding author: nadia@uitm.edu.my

Also, as soon as the residual load-bearing capacity of the corroded element reaches the applied load, the mechanism of failure can occur. For example, the partial collapse of the prestressed-precast roof structure of the Berlin Congress Hall in 1980 was primarily due to the severe corrosion of steel tendons (Helmerich & Zunkel, 2014).

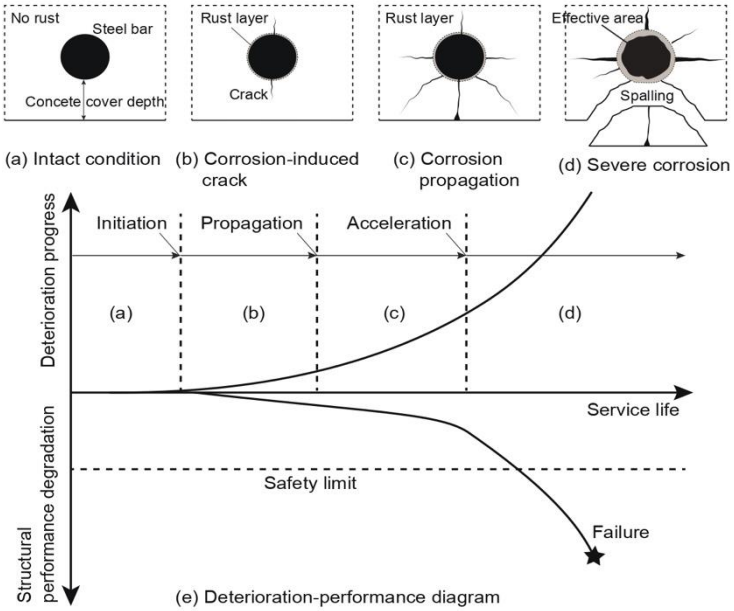

Fig. 1 - Conceptual view of the deterioration progress (Modified diagram from JSCE (2007))

The importance of understanding the effects caused by corrosion is essential. Corrosion can be described as an electrochemical process that involves the flow of positive and negative charges. Three elements must be present; (a) at least two locations on the steel bar having a different energy level (anode and cathode), (b) an electrolyte (pore water in concrete), and a metallic connection (steel bar itself). The ferrous steel at the anode location releases ferrous ions (Fe^{2+}) and electrons ($2e^-$) in which the freed electrons react with pore water content and oxygen and produce hydroxyl ions OH^-, which subsequently react with the ferrous ions and form ferric hydroxide ($Fe(OH)_2$), which is aa rusted product. The rusting process (production of ferric hydroxide) can also be accelerated when chloride ions (Cl^-) penetrate the concrete, where the accumulated steel rust can occupy a volume several times larger than that of the original steel (Zaki Ahmad, 2006; Zu, Franchois & Liu, 2017; Tian et al., 2023). This additional volume inevitably causes hairline cracks at the early stage of corrosion (Fig. 1b) and severe spalling or delamination of concrete at the advanced corrosion stage (Fig. 1d). As such, the steel bar at its anodic locations undergoes cross-section loss.

On the other hand, carbonation imposes a detrimental effect on the alkaline environment of concrete. In this situation, the carbon dioxide (CO_2) reacts with the calcium hydroxide ($Ca(OH)_2$) of the concrete and reduces the pH level to as low as 8 (Ramezanianpour, 2000; Ji et al., 2010; Monkman, 2011). As a result, the thin layer of oxide film on the bar surface created during cement hydration causes severe damage, and steel passivity is subsequently reduced. Moreover, the exposed bar surfaces may undergo significant corrosion under chloride attack, due to contamination by mixing water, aggregates, and chloride containing admixtures. Chloride-free concrete can also be contaminated by airborne chloride ions when exposed to harsh environments, such as coastal areas.

Dissimilar to other studies that have investigated the effect of corrosion on the durability of RC infrastructures such as bridges, nuclear power plants, offshore structures, and so forth, the influence of material deterioration on the structural performance of concrete building structures is less appreciated in the literature (Biondini et al., 2011; Lau & Lasa, 2016; Moreno et al., 2015; Han et al., 2013). Therefore, the authors of this study have conducted extensive research on the durability of a 60-year-old precast prestressed concrete (PCaPC) building structure of a former Nandan town hall located in Awaji Island, Japan. Although the building was demolished in 2017, it had several distinct features; (a) it was the first building of its type in Japan, constructed in 1957, (b) it was situated close to the coastal area and was subsequently exposed to the corrosive prone environment, and (c) it had experienced several earthquake shocks such as the destructive earthquake of Hanshin-Awaji earthquake in 1995.

Accordingly, the research conducted in this study consisted of two parts. Field and laboratory work on the deterioration of materials from the building was conducted, followed by analytical works on the deterioration of the building due to the influence of aging on the seismic performance of the building itself. In this study, the results of the first part, (i.e., carbonation, chloride content determination, and reinforcement corrosion state), are presented and discussed. The second part of this research will be published elsewhere.

2. Research Scope and Methods

This study investigates the former Nandan town hall, as shown in Fig. 2 (Kamaruddin et al., 2018). Originally, the structure of the town hall was a 3-story PCaPC building. The location of the building is illustrated in Fig. 3. The building was constructed in 1957 and was the first building in Japan to incorporate PCaPC beam elements. The building structure consisted of two reinforced concrete (RC) moment-resisting frames with nine 5-m bays in the longitudinal direction. In the transverse direction, the load-bearing structure of the building consisted of six moment-resisting frames with 11-m long PCaPC beams and four RC frames with RC walls along the staircases. The locations of the beams, columns, and walls on each floor are shown in Fig. 4. Other structural details of the building can be found in Ref. Kamaruddin et al. (2018).

Fig. 2 - Front view of former Nandan Town Hall

Fig. 3 - Location of the former Nandan Town Hall (QGIS opensource)

As shown in Fig. 3, the building was located in the vicinity of the coastal area at a distance of 350 m. According to the Japan Meteorological Agency (JMA), the accumulated average of precipitation that occurred between 1979 and 2016 was approximately 1288 mm/yr, with recorded temperature variation reaching as high as 37 ºC in summer and as low as -4 ºC in winter. The northerly wind averages around 14.5 km/h and is the predominant wind across the island. Several earthquakes between 1960 and 2016 have struck the target zone, mainly in the Minami Awaji area (plotted in Fig. 5). The massive Hyogo-ken-Nanbu earthquake in 1995 also struck this zone. Remarkedly, immediately following the earthquake, an extensive inspection was undertaken on the structure of the building, with no noticeable damage reported (GBRC, 1995).

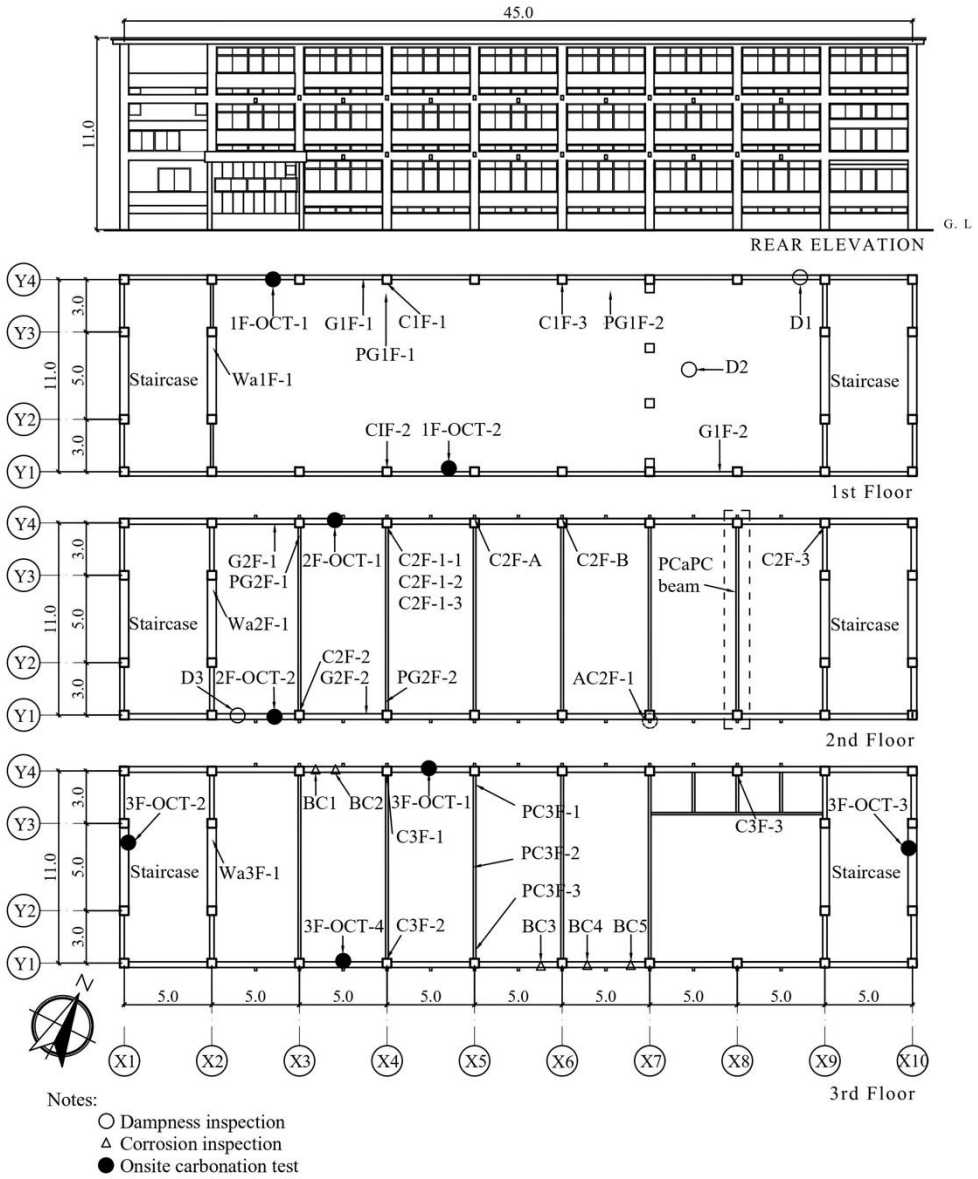

Fig. 4 - Elevation and floor plans (unit: m)

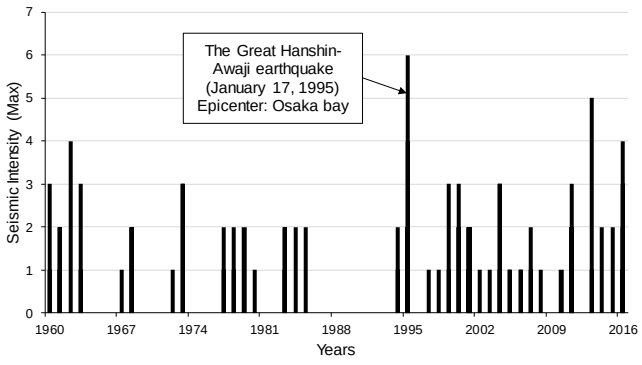

Fig. 5 - Recorded seismic intensities in Awajishima (Source: JMA)

In this study, field inspection and laboratory tests were conducted. The field inspection was covered on a drawing check to verify the existing building with the available drawings from the original design report. As the building was constructed in the early 1950s, the drawings of the building's architecture were hand-traced, and some details were missing. Therefore, before demolishing the building, extensive in-situ inspections were carried out. The reinforcement layout of the beams, columns, and walls was verified against the drawings via the electromagnetic wave radar scanning

(non-destructive method) and partial concrete removal (destructive method), respectively. However, this form of the inspection was not conducted in some inaccessible areas of the building, especially on the ceiling structure of the third floor. Hence, detailed checking was performed while demolishing the building.

Next, damage inspection was extensively carried out by a detailed visual observation on the principal cracks in structural elements. Laboratory tests were conducted to investigate the carbonation, chloride ion content, and mechanical properties of the structural elements. The carbonation depth of the beams, columns, and walls, 22 concrete core samples were collected from some of the elements on each floor. The locations of the sampling are shown in Fig. 5. The carbonation test was performed in accordance with JIS A 1152 (JSA, 2011). The concrete cores also were tested for compression based on JIS A 1108 (JSCE, 2007). The carbonation depth results were then verified against the carbonation depth prediction models recommended by Kishitani, JSCE, and RILEM (JSA, 2006; Sarja & Vesikari, 1996; Kishimoto et al., 2005). In these models, the carbonation depth is related to the square root of time. The equations of these models are as given below.

- Kishitani Model:

$$t = \begin{cases} \dfrac{0.31(1.15 + 3\,W/C)}{R^2\,(W/C - 0.25)}\,Y^2 & \mathrm{W/C} \geq 0.6 \\ \left[\dfrac{7.2}{R^2(4.2\,W/C - 1.762)}\right]Y^2 & \mathrm{W/C} \leq 0.6 \end{cases} \quad (1)$$

Where Y = carbonation depth (unit: cm), W/C = water-cement ratio, R = coefficient based on cement, aggregate, and admixture types (here R = 1).

The water-cement ratio of the RC elements and PC beams were assumed at 0.6 and 0.4, respectively.

- JSCE Model:

$$t = \left(\frac{1}{-3.57 + 9.0\,W/C}\right)^2 Y^2 \quad (2)$$

- RILEM 130 Model:

$$t = \left(\frac{Y}{c_{env}c_{air}af_{cm}^{b}}\right)^2 \quad (3)$$

Where c_{env} = environmental coefficient (c_{env} =0.5, structures exposed to rain) c_{air} = air content coefficient (here, c_{air} = 0.7, air entrained) , f_{cm} = standard compressive strength, and a, b = proportional constants (here, for Portland cement a = 1800 and b = -1.7) (Kishimoto et al., 2005).

The concentration of total chloride ion in the concrete members of the building was next determined by a potentiometric titration method in accordance with ASTM C 1152 (ASTM, 2004). Importantly, the total chloride or acid-soluble chloride in concrete depends on the chloride content of its ingredients such as cement, aggregate, and water. However, the precise amount of chloride that is contributed by each of these ingredients is difficult to define, given that the chloride contents in aggregate and in the concrete mixture are not equally distributed (Al-Saleh, 2015). As a result, the chloride levels of the columns (C2F-A and C2F-B), the PC beams (PC3F-1, PC3F-2, and PC3F-3), PC anchorage concrete cover (AC2F-1), and the grout of PC tendons were examined. The locations of material sampling are shown in Fig. 4. Initially, the collected concrete samples were pulverized into a fine powder (less than 800 μm). The equivalence point was then determined by the titration process. The total chloride content was obtained as expressed in Eq. (4) below.

$$Cl(\%) = 3.545\,[(V1 - V2)N]/W \quad (4)$$

Where $V1$ and $V2$ = equivalence points of the $AgNO_3$ solution used in the sample and blank tests, respectively (in milliliters). N = normality of the $AgNO_3$ solution, and W = mass of the sample portion (in grams).

The mechanical properties were investigated by the compression test and tensile test. The compression test results were compared with the designed strength of concrete of this building which is 17 MPa for RC and 49 MPa for PC. Samples of PC steel rods, reinforcing bars, and shear reinforcement, as shown in Fig. 7 were subjected to a tensile test. Distortion of the steel bar was measured by the attached strain gauge.

Fig. 7 - Samples of (a) PC steel rods; (b) column RC bars; (c) shear reinforcement

3. Results and Discussion

3.1 Field Inspections

3.1.1 Drawing Check Before Building Demolishing

The inspections of a demolished concrete column are illustrated in Fig. 8a. As expected, there were some discrepancies between the available drawings and actual reinforcement detailing. Initially, the thickness of concrete cover was estimated based on a standard value, 35-40 mm as shown in Fig. 8b. However, it was detected to be 100 mm from the on-site investigation. Fig. 8c shows the correction of the concrete cover thickness in the detail drawings. Furthermore, the column rebar as described in the original design report matched with the actual rebar detailing on the matter of its size and arrangement.

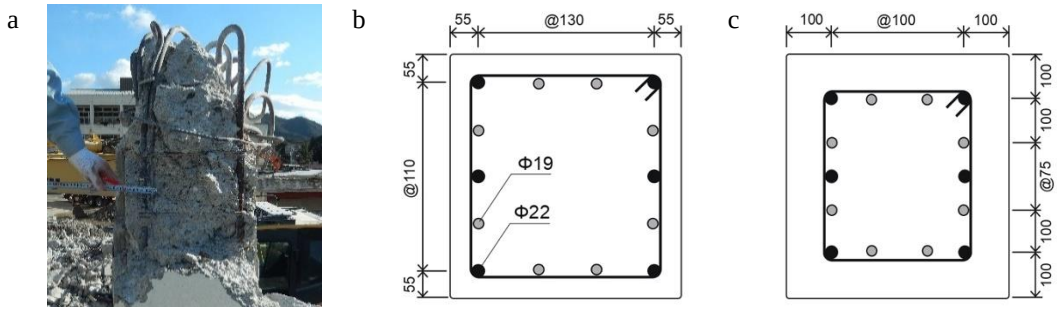

Fig. 8 - Reinforcement check and result (a) on-site demolished column; (b) estimated standard detailing; (c) actual detailing

3.1.2 Damage Inspections

On most of the columns, several flexural cracks at roughly similar intervals were observed, with crack widths ranging between 0.4 mm and 2.0 mm. The crack pattern of one column on the third floor is marked, as shown in Fig. 9a. Some flexural cracks of 0.40 mm width (maximum) were also observed in the RC beams, as marked on the RC beam of the first floor (Fig. 9b). It appears that these cracks occurred mainly due to lateral earthquake-driven deformations. No cracks were observed in the PCaPC beams and RC walls. Additionally, some corrosion-induced cracks and concrete spalling were observed at different locations on the spandrel walls, as shown in Fig. 9c and 9d; the concrete cover of these walls was approximately 35 mm. According to the deterioration diagram (Fig. 1), the steel corrosion in these walls exceeded the propagation stage. It should also be noted that the average concrete cover in the columns was 100 mm.

Fig. 10 shows the corrosion state of an anchorage mechanism and tendon of one of the PCaPC beams. Several anchorages were found densely covered with rust products, especially on the rear side of the building due to damage of the cover concrete (Fig. 10d). The rust extended to the couplers and tendons inside the aluminium sheath (Fig. 10b) and the grout material and aluminium sheath were severely deteriorated, as shown in Fig. 10c. The chloride content of the grout material was also examined. As discussed in this section, chloride levels were above the threshold limit, therefore implying a “propagation” state of corrosion.

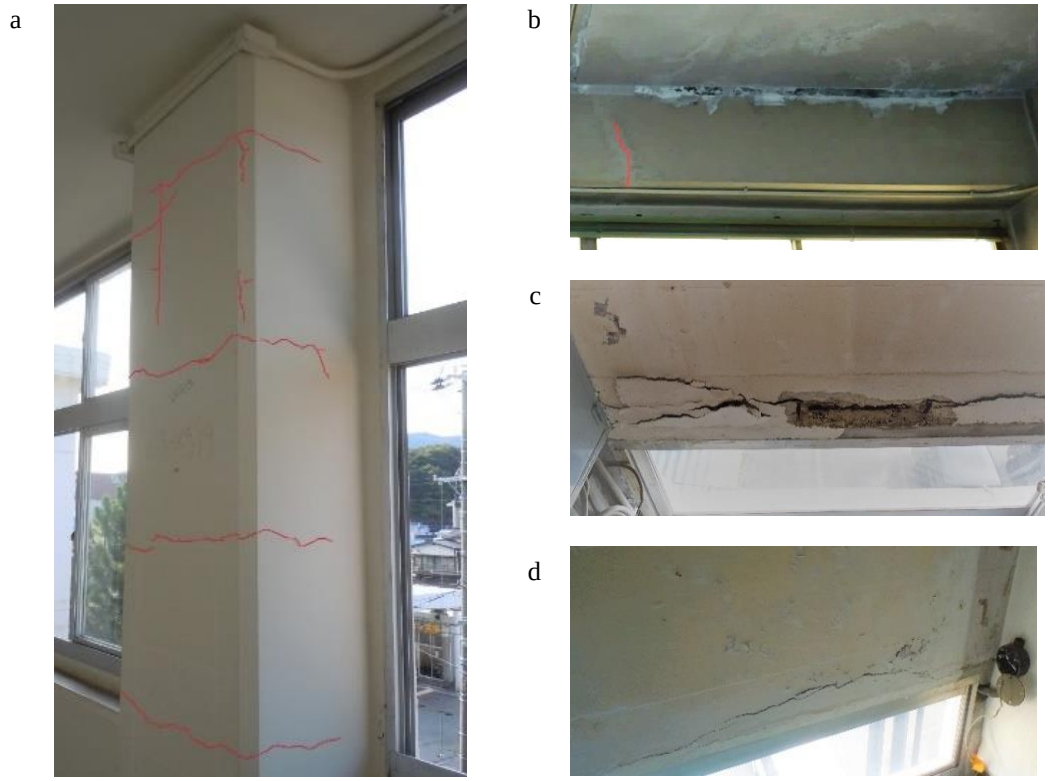

Fig. 9 - Visible crack patterns *(a) Column's flexural crack (third floor);* (b) RC beam's flexural crack (first floor D1); (c) Concrete spalling due to severe corrosion (third-floor spandrel wall BC3); (d) Corrosion-induced crack (third-floor spandrel wall BC4)

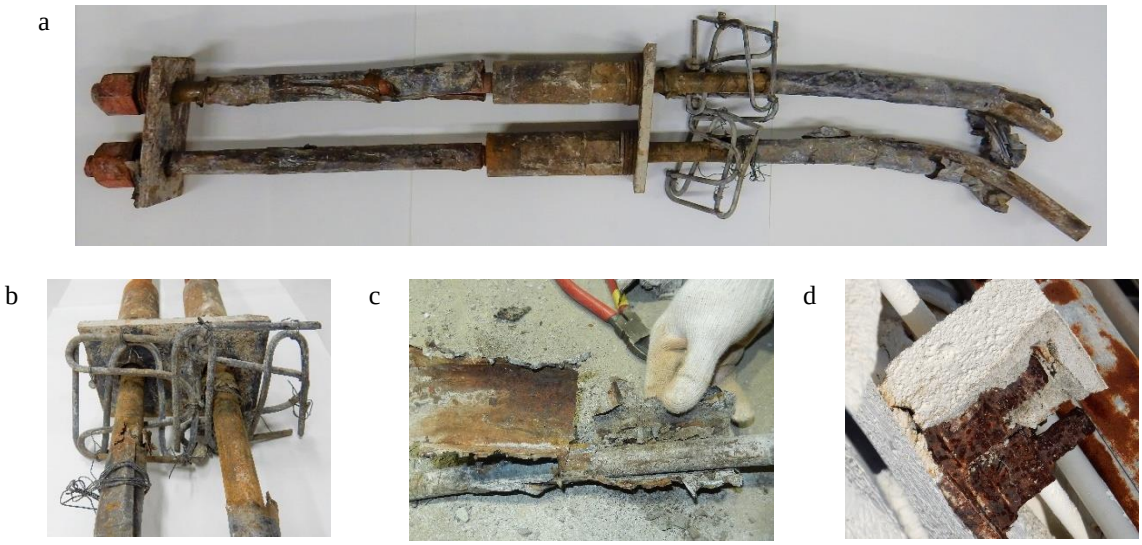

Fig. 10 - Observed corrosion in PCaPC beams (a) Corroded anchorage mechanism; (b) Tendon corrosion; (c) Corroded sheath and deteriorated grout; (d) Exposed anchorage

3.2. Laboratory Tests

3.2.1 Carbonation Test

Fig. 13a and 13b show a core concrete sample and its carbonation depth following spraying the solution on the fresh concrete surface of its split section, respectively.

a b

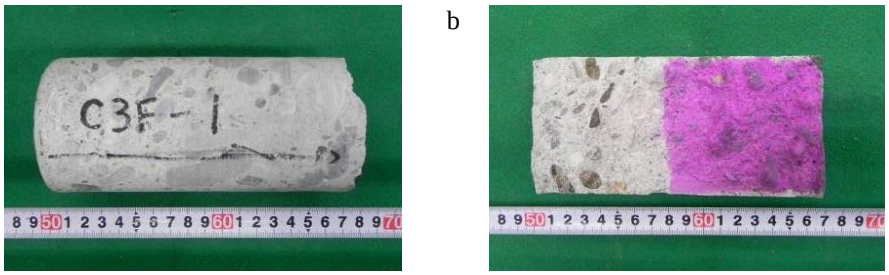

Fig. 13 - Carbonation depth indication on column core concrete (C3F-1) (a) before; (b) after

Table 1 - Carbonation depth results

Story	Member	Specimen	Carbonation depth (mm)		Cover depth (mm)	Model prediction/Avg. test		
						Kishitani	JSCE	RILEM
			Avg.	Max				
1	Column	C1F-1	7.5	8.5	100	3.47	18.67	22.67
		C1F-2	9.8	16.5	100	2.65	14.29	17.35
		C1F-3	14.2	16.0	100	1.83	9.86	11.97
	Shear wall	Wa1F-1	69.4	71.0	35	0.37	2.02	2.45
	RC beam	G1F-1	92.0	93.5	52	0.28	1.52	1.85
		G1F-2	5.0	26.5	52	5.20	28.00	34.00
	PC beam	PG1F-1	1.7	4.5	40	2.65	21.76	4.18
		PG1F-2	2.4	4.0	40	1.88	15.42	2.95
2	Column	C2F-1-1	50.0	52.5	100	0.52	2.80	3.40
		C2F-1-2	41.1	45.5	100	0.63	3.41	4.14
		C2F-1-3	68.1	70.5	100	0.38	2.06	2.50
		C2F-2	65.6	68.0	100	0.40	2.13	2.59
		C2F-3	29.1	34.5	100	0.89	4.81	5.84
	Shear wall	Wa2F-1	69.4	73.0	35	0.37	2.02	2.45
	RC beam	G2F-1	51.9	54.0	52	0.50	2.70	3.28
		G2F-2	38.9	41.5	52	0.67	3.60	4.37
	PC beam	PG2F-1	0.5	2.5	40	9.00	74.00	14.20
		PG2F-2	2.5	6.0	40	1.80	14.80	2.84
3	Column	C3F-1	76.5	79.0	100	0.34	1.83	2.22
		C3F-2	71.6	73.5	100	0.36	1.96	2.37
		C3F-3	77.5	80.5	100	0.34	1.81	2.19
	Wall	Wa3F-1	22.4	35.0	35	1.16	6.25	7.59

The measured average depths of concrete carbonation of collected samples were as shown in Table 1. The relationship between the carbonation depth and the cover depth of each element is plotted in Fig. 14. As can be seen in the figure, in most cases, the carbonation did not exceed the cover depth. In other words, it can be implied that during these 60 years of service, the confining concrete sustained the alkali environment for the steel reinforcements and did not contribute significantly to the corrosion.

Notably, if the building were designed for the conventional cover depth (30-40 mm), serious corrosion due to the reinforcement depassivation would be very likely to occur (Teplý, 2002). Also, the PCaPC beams had the smallest carbonation depth values which could be attributed to the relatively low water-cement ratio and low concrete porosity of high strength concrete (Fattuhi, 1986). From Table 1, it is evident that the lower floors experienced less severe carbonation.

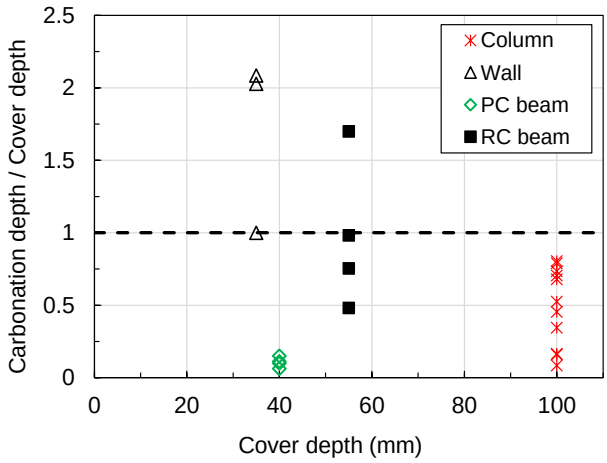

Fig. 14 - The ratio of carbonation depth to cover depth

3.2.2 Carbonation Depth Prediction

The models recommended by Kishitani, JSCE, and RILEM have been used to compare the model predictions vs. the experimental results. The parabolic curves predicted by the model vs. the test results are plotted in Fig. 15.

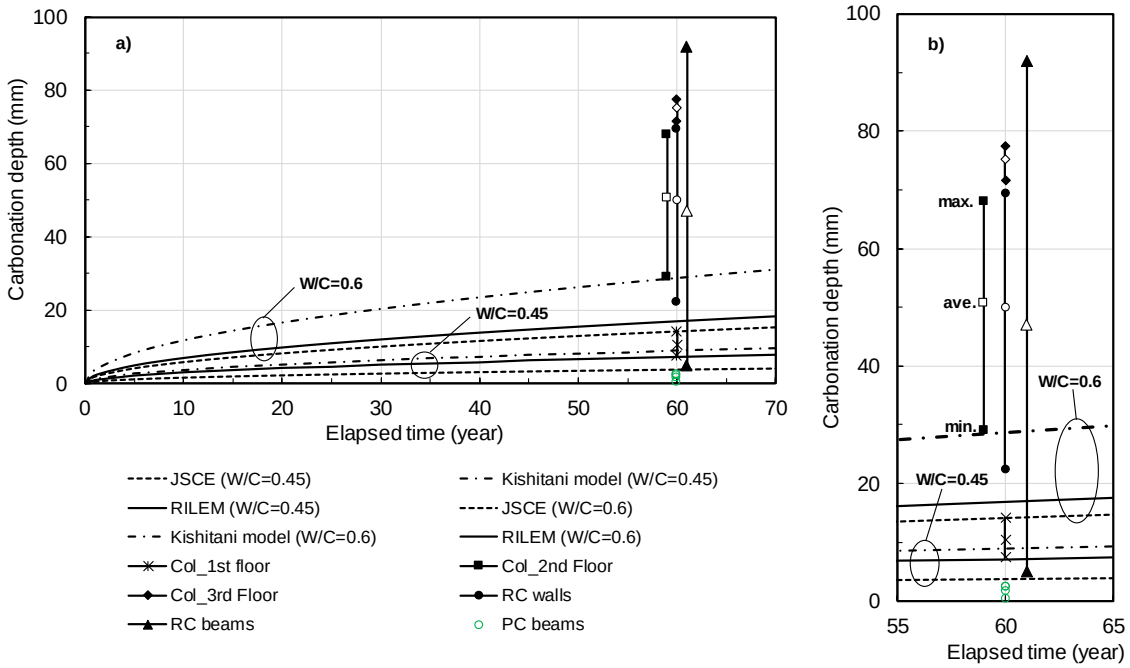

Fig. 15 - Carbonation depth prediction vs. test results

Notably, the critical parameter in the employed carbonation depth models, as mentioned above, is the water-cement ratio. These ratios were approximated as W/C = 0.60 for the RC beams, shear walls, and columns, and W/C = 0.45 for the PC beams based on the design compressive strength in this study. As such, the larger the W/C ratio, the higher the carbonation depth is predicted. The ratio of predicted values over the test results are listed in Table 1. For a better comparison, the test results and the model curves are plotted in Fig. 15a and 15b. As shown in the figures, the average values obtained from the W/C = 0.6 samples have tremendously exceeded the model predictions. Moreover, the distinct discrepancies between the maximum and the minimum measured values should be noted.

On the other hand, the measured carbonation depth values of W/C = 0.45 PC beams were smaller compared to those of the model predictions. Among the three employed models, the JSCE model predicted less conservative values regarding the maximum measured values of the PC beams. Also, given there were no previous records regarding the carbonation depth of different members of the building during its service life available, the validity of the model predictions over an extended time cannot be judged accurately. Therefore, special care is needed for forensic assessments based on model predictions.

3.2.3 Chloride Ion Content

The results of the total acid-soluble chloride content tests are depicted in Table 2. Based on JSCE 2007, the threshold limit of chloride content is 1.2 kg/m^3 (JSCE, 2007). The PC grout samples collected and the anchorage cover were found to contain a tremendous amount of chloride content, which was mainly attributed to the airborne chloride concentration under the influence of the adjacent coastal area. Furthermore, it appears that the relatively high permeability of the anchorage cover and the formation of cracks during the service life attributed to the extension of chloride content into the grout of the PC tendons. Such chloride attacks could partially contribute to the corrosion of tendons, as shown in Fig. 10. The high concentration of chloride ion content was also observed at the PC beam ends and the outside cover concrete of the columns. Although the concrete inside the building was not diagnosed with chloride ion content above the prescribed threshold limit.

Table 2 - Measured total acid-soluble chloride content

Sample location	Total acid-soluble chloride content		Test results/ threshold
	Percent by mass of concrete	kg/m^3	
RC col. (C2F-A), outside face*	0.105	2.313	1.928
RC col. (C2F-A), inside face*	0.049	1.079	0.899
RC col. (C2F-B), outside face	0.218	4.800	4.000
RC col. (C2F-B), inside face	0.021	0.463	0.386
PC beam (PC3F-1)	0.098	2.159	1.799
PC beam (PC3F-2)	0.021	0.463	0.386
PC beam (PC3F-3)	0.126	2.775	2.313
Anchorage cover (AC2F-1)	0.274	6.035	5.029
PC tendon grout	0.346	5.195	4.329

* Outside face of the concrete is exposed to the environment outside the building and the inside face is exposed only to the indoor environment.

3.2.4 Mechanical Tests

Structural analysis was conducted based on the design strength and the actual mechanical properties after 60 years of service life. Mechanical tests on the concrete and steel materials collected from the building were performed according to JIS A 1108 and the results are shown in Table 3 and 4, respectively (JSA, 2006). Notably, the average compressive strengths of the core samples from the selected column on the first floor and the RC wall on the third floor were approximately 10% smaller compared to the compressive design strengths of 17.7 MPa. Similarly, the average measured yield strengths of the collected longitudinal and transverse reinforcements of the columns were beneath the design yield strength of 392 MPa.

Table 3 - Mechanical properties of core concrete samples

Story	Member	Compressive strength		Young's Modulus (kN/mm^2)
		(N/mm^2)	Measured/design	
1	RC column	16.3	0.92	14.8
	RC wall	21.4	1.21	-
	RC beam	34.8	1.97	-
	PC beam	70.7	1.44	33.4
2	RC column	22.5	1.27	22.1
	RC wall	19.9	1.12	-
	RC beam	25.3	1.43	
	PC beam	65.3	1.33	35.8
3	RC column	22.9	1.29	21.1
	RC wall	16.0	0.90	-

Table 4 - Mechanical properties of collected steel bar samples

Member	Visible corrosion	Diameter (mm)	Yield strength		Elastic Modulus (kN/mm^2)	Tensile strength (N/mm^2)
			(N/mm^2)*	Measured/design		
PC rod	slight	24.10	850	1.57	186	995
Column main reinforcement	slight	19.40	313	0.79	160	482
Hoop	severe	8.76	265	0.67	203	503

*** 0.2% offset**

4. Conclusions

An extensive investigation was conducted on a 60-year-old PCaPC building structure that had been exposed to the corrosion-prone environment and had also been struck by a massive earthquake in 1995, having an intensity of 6. Several other earthquakes also occurred following this period. The following findings are summarized into two distinct categories, namely field and laboratory investigations.

a) Field Investigation

- From the visual inspection of the building, a minor flexural crack on the columns and walls was observed ranging between 0.4 and 2.0 mm. However, no cracks were detected on all PCaPC beams.
- Severe corrosion-induced cracks on the wall were observed on the third floor.
- PC anchorages were found to be severely corroded, especially on the second floor. The rust from anchorage was detected to have extended to the PC system.

b) Laboratory Investigation

- From the compression test on the concrete cores, all samples met the design compressive strength, especially on the second floor, except for the column and wall samples on the first and second floors.
- Carbonation depths were significant on the sampled columns and walls, especially on the third floor. The carbonated zone extended to the reinforcing steel where corrosion was imminent, however, the PC beams were only affected by a small depth of carbonation.
- Among the three suggested prediction models (Kishitani, JSCE, and RILEM models), the JSCE model underestimated the carbonation depth compared to the other two models for both W/C types 0.6 and 0.45. However, the carbonation depth of the PC beams was detected to be on the safe side of the predicted carbonation depth. Furthermore, the validity of the model prediction could not be judged accurately, given the unavailability of data during the building's service life.
- According to the potentiometric test in determining the chloride ion content in concrete and cement, the amount of chloride ion on the concrete surface inside the building was 85%, almost reaching the threshold limit value of 1.2 kg/m^3 stipulated by JSCE. A high amount of chloride ions was found on the PCaPC beam system at the anchorage concrete cover, grout, and both ends of the PC beam. Those chloride ions greatly exceeded the threshold limit, especially on the anchorage concrete cover and grout. Heavy rust was also observed on the number of PC beam anchorages at the rear of the building. Likewise, the tendon and sheath were found covered with a thin layer of rust, and grouting faults (air-filled voids) inside the duct of bonded steel tendons were also detected.

In conclusion, based on the field and laboratory investigation that was performed, it can be concluded that the first PCaPC building structure have substantially satisfied structural performance during its service life of 60 years, even though a massive earthquake had struck the building which had also undergone signs of deterioration due to aging. As a consequence, the high performance of PC buildings (especially in Japan) has been well recognized, especially given their ability to resist high seismic activities following the Hyogo-ken-Nanbu earthquake event in 1995.

Acknowledgement

The authors would like to acknowledge Minami-Awaji City council, CONSTECH and the General Building Research Corporation of Japan (GBRC) team for the constant support, collaboration and strong cooperation.

References

Al-Saleh S. A. (2015). Analysis of total chloride content in concrete, Case Stud. Constr. Mater., vol. 3, no. November 2002, pp. 78–82

ASTM (2004), ASTM C1152: Standard Test Method for Acid-Soluble Chloride in Mortar and Concrete, American Society for Testing Materials, vol. 15, no. 5. p. 4

Biondini F., Palermo A., and Toniolo G. (2011). Seismic performance of concrete structures exposed to corrosion: Case studies of low-rise precast buildings, Struct. Infrastruct. Eng., vol. 7, no. 1, pp. 109–119

Fattuhi N. I. (1986) Carbonation of concrete as affected by mix constituents and initial water curing period, *Mater. Struct.*, vol. 19, no. 2, pp. 131–136

Gao Y., Zheng V., Zhang J., Xu S., Zhou X., and Zhang Y. (2019). Time-dependent corrosion process and non-uniform corrosion of reinforcement in RC flexural members in a tidal environment, Constr. Build. Mater. vol. 213, pp. 79–90

GBRC, Seismic Diagnosis Survey Report of Nandan Town Office Building, Osaka, Japan, 1995.

Hamada H. *et al.* (2003). A study on environmental conditions affecting long term deterioration of concrete structures in japan, in Our World in Concrete & Structures, pp. 97–114.

Han S. H., Park W. S., and Yang E. I. (2013) Evaluation of concrete durability due to carbonation in harbor concrete structures, Constr. Build. Mater., vol. 48, no. November 2013, pp. 1045–1049

Japanese Standard Association (JSA) (2011). Method for measuring carbonation depth of concrete JIS A 1152. JSA, Tokyo

Japanese Standard Association (JSA) (2006). Method of test for compressive strength of concrete JIS A1108, JSA, Tokyo

Japan Society of Civil Engineers (JSCE) (2007). Standard specifications for concrete structures "Design," no. 15. Tokyo, Japan, 2007.

Japan Society of Civil Engineers (JSCE) (2007). Standard specifications for concrete structures "Design," no. 15. Tokyo, Japan, 2007.

Ji Y., Yuan Y., Shen J., Ma Y., and Lai S. (2010) Comparison of concrete carbonation process under natural condition and high CO2concentration environments, J. Wuhan Univ. Technol. Mater. Sci. Ed., vol. 25, no. 3, pp. 515–522

Kamaruddin N., Watase C., Raouffard M. M., Bedriñana L. A., Zhang K., and Nishiyama M. (2018) Durability and Seismic Resistance of an Aged Precast Prestressed Concrete Building Based on Field Inspections and Laboratory Testing, in High Tech Concrete: Where Technology and Engineering Meet, Cham: Springer International Publishing, pp. 2256–2265.

Kishimoto Y., Hokoi S., Harada K., and Takada S. (2005) Prediction Model For Carbonation of Concrete Structure Considering Heat and Moisture Transfer, J. Struct. Constr. Eng. - AIJ, no. 595, pp. 17–23

Lau K. and Lasa I. (2016). Corrosion of prestress and post-tension reinforced-concrete bridges, in Corrosion of Steel in Concrete Structures, pp. 37–57.

Li K., Chen Z., and Lian H. (2018). Concepts and requirements of durability design for concrete structures: an extensive review of CCES01, Mater. Struct., vol. 41, no. 4, pp. 717–731

Monkman S. (2016). TECHNICAL NOTE - Types of Concrete Carbonation Early age carbonation, CarbonCure Technol

Moreno J. D., Bonilla M., Adam J. M., Victoria Borrachero M., and Soriano L. (2015). Determining corrosion levels in the reinforcement rebars of buildings in coastal areas. A case study in the Mediterranean coastline, Constr. Build. Mater., vol. 100, pp. 11–21

Ramezanianpour A. A., Tarighat A., and Miyamoto A. (2000). Concrete Carbonation Modelling and Monte Carlo Simulation Method for Uncertainty Analysis of Stochastic Front Depth, Mem Fac Eng Yamaguchi Univ, vol. 50, 2, no. 149, p. (149)57-(152)60

Sarja A. and Vesikari E. (1996). Durability Design of Concrete Structures

Sosa M. *et al.* (2011). Influence of the marine environment on reinforced concrete degradation depending on exposure conditions, Int. J. Electrochem. Sci., vol. 6, no. 12, pp. 6300–6318

Teplý B. (2002). Modelling of Deterioration Effects on Concrete Structures, Acta Polytech., vol. 42, no. 3

Tian Y., Zhang G., Ye H., Zeng Q., Zhang Z., Tian Z., Jin X., Jin N., Chen Z., Wang J. (2023) Corrosion of Steel Rebar in Concrete Induced by Chloride Ions Under Natural Environments, Construction and Building Materials., vol 369

Zhu W. and François R. (2014). Corrosion of the reinforcement and its influence on the residual structural performance of a 26-year-old corroded RC beam, Constr. Build. Mater., vol. 51, pp. 461–472

Zhu W., François R., and Liu Y. (2017). Propagation of Corrosion and Corrosion Patterns of Bars Embedded in RC Beams Stored in Chloride Environment for Various Periods, Constr. Build. Mater., vol. 145, pp. 147–156